

Chapter 6

Outline of Future Plasma Models of the Solar Atmosphere and its Activity

We wish to synthesise the spectral observations by combining the atomic model of ADAS with a suitable plasma model. Cross-comparison with the instrumental measurements will allow progress to be made in defining realistic physical mechanisms for many of the observable solar features. SOHO is essentially a quiet sun observing station. However, it is clear that plasma dynamics play a significant role in prominence formation, x-ray bright points, sunspot activity and possibly also coronal heating. It is our intention to adopt a numerical hydrodynamic model that will allow us to investigate some of these phenomena. From the model we will obtain temperature, density and velocity information within a pre-defined plasma geometry that we can use in the production of $G(T_e, N_e)$ functions. Thus we can build up a time development of the atomic model that can be related to the expected evolution of some solar feature by the simulation of the hydrodynamic behaviour. Clearly it is an enormous computational task to develop a code separately and seems unnecessary when so many are currently in use. The most widely available, at present, are for computing solar flare loop hydrodynamics. Therefore, we obtained a copy of the flare hydrodynamic loop code of Peter MacNeice (1983) to use as a starting point. It has certain special

advantages discussed below.

Solar flares are not observable with SOHO, except through whole sun images such as those of EIT (Extreme Ultraviolet Imaging Telescope). Indeed, the detector saturation limit, of an instrument such as SUMER, is so low that flare enhanced lines would destroy it. This is in fact already a problem for bright lines such as Lyman α . As a result, it is not our intention, at least for planned SOHO observations, to attempt to develop the modelling duration or physical reality of the MacNeice code for flares. Our aim is to explore the applicability of the loop model to other plasma dynamics and energy balance questions such as prominence condensations (Antiochos & Klimchuk(1990)) or impulsive heating (Spadaro, Lanza & Antiochos (1996)). However, it was necessary to investigate the physical assumptions of the MacNeice model to see whether this could be done. Here we review the development of the physical basis for producing this type of numerical flare model. We also present results from a test run of the code and offer suggestions for future work. Finally, the concluding remarks of the thesis are presented.

6.1 Relevant Literature

EUV, XUV and X-ray observations by ground and space based instrumentation have shown that magnetic loop arcades dominate the observed structures of the low corona. This is as expected from an empirical view of the global processes contributing to energy transport from the solar interior to the atmosphere. We know that thermonuclear fusion takes place in the core of the sun, and that the nuclear furnace converts hydrogen into helium. The resulting energy released in each reaction is radiated outward towards the solar surface. As the temperature decreases towards its minimum, at the top of the solar photosphere, $\sim 10^7 K \rightarrow 4400K$, the free electrons of the highly stripped ions begin to recombine in the plasma. As a consequence, the escaping photons are more readily absorbed by the atoms and ions. Therefore, the plasma becomes optically thick and unstable, resulting in the appearance of large convection currents which transport the energy to the surface. Evidently, the permeating magnetic field lines are 'rolled up' into fluxtubes as the giant convection cells rise and fall. These

magnetic loops break through the surface of the chromosphere and into the corona.

In the low corona the ratio of the plasma pressure to the magnetic pressure, generally called β , is less than one (Spruitt(1981)). As a result, the plasma particles are confined to motion along the magnetic field lines. It is thus possible to model the hydrodynamic behaviour of a plasma by assuming that it moves along a one dimensional magnetic flux tube. The geometrical configuration of the tube is an open parameter. For flare modelling it is usual to assume that the loop structures, observed in the corona, are almost symmetrical semi-circles. If this assumption is made, it is sufficient to model one half of the loop. For models of suspended material in magnetic fields, it has been suggested (Poland, Mariska & Klimchuk (1986)) that a semi-circular loop with a long shallow symmetric dip is useful. Alternatively, for bright points and jets, a vertical flux tube may be all that is necessary. In any case, the principle is to model the evolution of the plasma in the tube, in response to some perturbation (perhaps an energy injection), by solving the equations of plasma transport theory. It is convenient here to rederive the equations of mass continuity, momentum conservation and energy balance.

6.1.1 Plasma Fluid Equations

To model a plasma it is necessary to know the distribution functions of all the particles. We denote these distribution functions by $f(\mathbf{x}, \mathbf{v}, t)$. At this stage we do not distinguish between the particle species. The function gives the particle density distribution at the position (\mathbf{x}, \mathbf{v}) in velocity space, where \mathbf{x} is the (x, y, z) coordinate of the particles, and \mathbf{v} are their velocities in each direction, i.e. (v_x, v_y, v_z) . $f(\mathbf{x}, \mathbf{v}, t) dx dy dz dv_x dv_y dv_z$ is then the particle density within the six dimensional volume element $d\mathbf{x}d\mathbf{v}$. In general, the particles in the plasma will move towards a Maxwellian distribution of velocities (eq. 2.1). A discussion of how quickly this process takes place is given in sec. 2.1.2. For a discussion of the influence of a non-Maxwellian tail in the electron distribution function in solar atmospheric models see MacNeice, Fontenla & Ljepojevic(1991). We restrict our present discussion to particle distributions that are Maxwellian.

If we could sample the particle distribution functions at every point in the plasma we would obtain a complete description of the plasma state. In reality this is not possible. However, we can acquire useful quantities by taking velocity moments of the distribution function.

$$\text{moment } i = \int f(\mathbf{v})v^i d^3\mathbf{v} \quad (6.1)$$

Taking moments for $i = [0, \infty]$ would allow us to completely determine the distribution function but it is usually only necessary to investigate the lower order moments. There is a problem which occurs through taking increasing moments. Each successive one introduces the next higher order moment and at some stage an assumption must be made that will allow us to ‘close’ the set of equations. Usually it is sufficient to set the third moment, that of thermal conductivity, to zero.

Returning to the model plasma and taking the first three moments, we obtain,

1. $\int f(\mathbf{x}, \mathbf{v}, t)d^3\mathbf{v} \equiv n(\mathbf{x}, t)$
2. $\frac{1}{n} \int f(\mathbf{x}, \mathbf{v}, t)\mathbf{v}d^3\mathbf{v} \equiv \mathbf{u}(\mathbf{x}, t)$
3. $m \int (\mathbf{v} - \mathbf{u})(\mathbf{v} - \mathbf{u})f(\mathbf{x}, \mathbf{v}, t)d^3\mathbf{v} \equiv \frac{3}{2}nk_B T$

where $n(\mathbf{x}, t)$ is the particle density, $\mathbf{u}(\mathbf{x}, t)$ is the mean particle velocity and $\frac{3}{2}nk_B T$ is the mean particle energy. We can obtain the plasma transport equations in analogous fashion by considering the Boltzmann kinetic equations,

$$\frac{\partial f}{\partial t} + \mathbf{v} \cdot \frac{\partial f}{\partial \mathbf{x}} + \frac{\mathbf{F}}{m} \cdot \frac{\partial f}{\partial \mathbf{v}} = 0 \quad (6.2)$$

This equation describes the evolution of the particle distribution functions. The Boltzmann equations are not specific to plasmas but can be made so by inclusion of the Lorentz force.

$$\mathbf{F} = q(\mathbf{E} + (\mathbf{v} \times \mathbf{B})) \quad (6.3)$$

The Lorentz force takes due account of the influence, on the particles, of the local magnetic and electric fields. From eqs. 6.2 and 6.3 we obtain,

$$\frac{\partial f}{\partial t} + \mathbf{v} \cdot \frac{\partial f}{\partial \mathbf{x}} + \frac{q}{m} (\mathbf{E} + (\mathbf{v} \times \mathbf{B})) \cdot \frac{\partial f}{\partial \mathbf{v}} = \left(\frac{\partial f}{\partial t} \right)_c \quad (6.4)$$

which is the Fokker-Planck equation. In fact this derivation assumes no particle interactions in the plasma. This provides no problem provided we neglect short range reactions and postulate that because the electric and magnetic fields, \mathbf{E} and \mathbf{B} , are due to all the other particles in the plasma, they adequately describe the particle interactions. This separation of long range and collisional interactions is only possible if plasma effects dominate over particle effects i.e. the plasma parameter, $\Omega = \frac{1}{n_\nu \lambda_D^3}$, is small, where n_ν is the particle density of the species ν , and λ_D is the debye length (i.e. the length at which a particles' potential is screened from the other particles in the plasma). The plasma parameter will be small if the Debye sphere surrounding the particle, contains large numbers of particles. This assumption is valid for the upper solar atmosphere (see MacNeice(1983)).

Taking moments of eq. 6.4 provides us with the fluid equations. These were originally derived by Braginskii(1965) and recent examples of the method were provided by Cuperman et al.(1981), Bittencourt(1986) and Elliot(1993). The resulting equations are,

$$\frac{\partial n}{\partial t} + \frac{\partial}{\partial \mathbf{x}} (n\mathbf{u}) = 0 \quad (6.5)$$

which is the equation of mass continuity,

$$mn \left(\frac{\partial}{\partial t} + \mathbf{u} \frac{\partial}{\partial \mathbf{x}} \right) \mathbf{u} = -\nabla p - \nabla \cdot \mathbf{P} + qn (\mathbf{E} + (\mathbf{v} \times \mathbf{B})) P_{ab} \quad (6.6)$$

which is the momentum conservation equation and

$$\frac{3}{2}nk_B \left(\frac{\partial}{\partial t} + \mathbf{u} \frac{\partial}{\partial \mathbf{x}} \right) T + \frac{\partial}{\partial \mathbf{x}} (p\mathbf{u}) + \frac{\partial}{\partial \mathbf{x}} (\mathbf{P}\mathbf{u}) = -\nabla q + Q_{ab} \quad (6.7)$$

which is the energy conservation equation. In these equations, \mathbf{P} is the stress tensor. The diagonal elements are the usual hydrostatic pressures, p , which have been separated out in eqs. 6.6 and 6.7. The off-diagonal elements represent the plasma viscosity and q is the heat flux, which is the next higher order moment. The term P_{ab} represents changes in the momentum density of the particles a , due to collisions with particles b . In eq. 6.7 the term Q_{ab} is the analogous expression for changes in the energy density due to collisions. This latter term can also include energy source and sinks, see sec.6.3.1.

6.2 Flare Loop Modelling: Background Literature

We focus here on the one dimensional symmetrical semi-circular loop problem. This approach was adopted for flare modelling by many workers in the early eighties. Interest was awoken due to the advent of the Solar Maximum Mission satellite. The energy balance, in the loop, is influenced by conduction, convection and radiation, and the plasma particles move under the control of gravity and the pressure gradients that develop. The flare energy is required to be conducted into the chromosphere where the higher densities can more easily radiate it away. Typically, authors adopted either a *Non-Thermal* or *Thermal* model. We describe briefly here the overall approach adopted for each model and the sorts of results obtained by the original modellers primarily to outline the results of the test (see section.6.3.1).

The non-thermal model investigated the coronal loops' hydrodynamic response to the injection of a highly energetic electron beam at the loop apex and was investigated by, for example, Nagai & Emslie(1984), MacNeice et al.(1984), Fisher, Canfield & McLymont(1985), Peres et al.(1987) and Mariska, Emslie & Li(1989). Essentially the model predicts that rising magnetic field lines break through into the corona and 'pinch' out plasmoids which they effectively carry upwards. Magnetic reconnection takes place in the wake of the rising material and the reconnection process produces electric fields which accelerate electrons spirally down the magnetic field lines. The electrons collide with ions as they go and emit thermal Bremsstrahlung before depositing the majority of their energy in the chromosphere by coulomb collisions. Brown (1973) coined the phrase *thick target* for the denser chromospheric collision point. Each of them assumed a power law distribution for the electron beam with a low energy cut-off point (usually 10-20keV).

All of the models of the authors mentioned above produced results that were qualitatively similar despite the differing energy inputs and durations (from repeated bursts of 1.8×10^{12} ergs $\text{cm}^{-2}\text{s}^{-1}$ every 2 secs. for 240s (Nagai & Emslie) to a 5 sec. burst of 3×10^{10} ergs $\text{cm}^{-2}\text{s}^{-1}$ for Fisher et al.). After the beam impacts on the chromosphere the temperature increases to that of the corona in less than a second. The plasma pressure increases and acts like a piston driving material up the

loop at speeds of up to $1,000\text{kms}^{-1}$. Consequently diminished upward velocities are seen. A cooler denser compression wave is generated that propagates deep into the chromosphere towards the photosphere at supersonic speeds. Fisher et al. named the upward plasma motion, *chromospheric evaporation*, and the downward compression, *chromospheric condensation*. As a result of the condensation a shock wave is formed that travels ahead of the compression wave eventually slowing due to the increasing pressure and density. The coronal material increases in temperature and density to $> 10^7\text{K}$ and $\sim 10^{12}\text{cm}^{-3}$ respectively. When the energy input ceases conduction and radiation act to re-establish the pre-flare atmosphere. The plasma in the low corona cools but the temperature and density at the loop top continues to increase principally due to the collision of the symmetric rising fronts. However, only the numerical model of Nagai & Emslie lasted long enough to model this event and this was partly due to the gross nature of the numerical grid they used compared with the others. Their model showed the atmosphere relaxing to its initial state by an oscillatory behaviour. As later pointed out by Gan, Fang & Zhang(1991) the collision of these symmetric fronts is extremely violent and results in drastic changes in the physical parameters. The collision causes a localised increase in temperature and density resulting in the formation of a new pressure peak which forces material back down the loop at hundreds of kms^{-1} . Their calculation terminated due to numerical instabilities associated with the ferocity of this collision. Clearly it would be interesting to follow this phenomenon more accurately.

The thermal model considered plasma motions initiated by heat fluxes from a high temperature thermal source deposited with a Gaussian distribution in the electrons at the loop top. Once again many authors investigated the problem. For example, Nagai(1980), Somov, Sermulina & Spektor(1982), Pallavicini et al.(1983), Cheng et al.(1983), MacNeice(1986), Kopp et al.(1986) and Gan et al.(1991). The source length was generally chosen so that the majority of the flare energy was deposited in the corona. An immediate temperature rise resulted causing a supersonic thermal wave to propagate down to the chromosphere. On arrival, it heats the cool chromospheric plasma. Subsequently the response is qualitatively similar to that of the non-thermal model i.e. a pressure peak develops which drives chromospheric evaporation and

condensation.

Resolution of the thermal wave entering the transition region is a major problem with these numerical models. For a chosen flare energy input of $2 \times 10^{11} \text{ erg cm}^{-2} \text{ s}^{-1}$ the minimum mesh spacing required is $\sim 10 \text{ cm}$. In addition, resolution of the steep temperature and density gradients that develop at the base of the transition zone is of concern. Prior to the work of MacNeice et al.(1984) this had always been insufficient. MacNeice(1986) achieved a resolution of under 100cm for the thermal wave front with their *adaptive regriding* technique which is outlines in section.6.3.1. Many of the other authors also developed such moving grids.

After the Solar Maximum Mission workshop in 1982 a flare dynamic modelling group was initiated to intercompare the various codes produced by the above authors. A *benchmark* calculation was defined against which all developing codes could be tested. Despite large discrepancies initially in some of the least sensitive parameters, for example the temperature at the loop top, close agreement was eventually achieved. The problem was of the thermal type and we use a modification of this as our test in section.6.3.1.

Many refinements to these models have been included to treat, for example, the problem of defining a realistic description of the conductive heat flux (MacNeice et al.(1984)) or particle return current effects (Karlicky & Henoux (1992)). Ultimately the aim of all the work was to use the models to predict observational signatures with critical differences that can be examined experimentally to discriminate between them. For example, Mariska et al.(1989) made a detailed examination of which ranges of electron beam parameters were better able to reproduce the observations. Much further research has also been undertaken in this area and much progress has been made during the lifetime of the YOHKOH satellite. However, we make no attempt to comment on the observational evidence or the numerical refinements here as the field of solar flare studies is enormous in itself and beyond the scope of our present work and this thesis.

6.3 MacNeice Flare Hydrodynamic Model

It is essential to develop confidence in the computer code before further developing it. This is non-trivial as it is likely that the code has been altered many times since its first use in 1983. To do this we have attempted to reproduce the results of the thermal conduction front model of MacNeice (1986). This should allow us to address the complexities of the adaptive rezoning techniques. This involves removing some of the more refined qualities of the code, produced in recent years.

6.3.1 The Benchmark Model

Essentially the problem was posed for the flare hydrodynamic modellers (see sec.6.2). We review here the parameters and expressions required for the original model and the necessary alterations we have made whilst maintaining the essence of the problem.

Our initial loop is slightly shorter than MacNeice used. This was dictated by the model atmospheres we obtained with the code. Thus the semi-circular symmetric loop has a length of $1.02 \times 10^9 \text{cm}$ and a cross-section constant in space and time. The effects of the curvature are ignored and this is justified since the ratio of the loop radius to internal radius is large, typically a factor 7 (Kopp et al.(1986)). The loop footpoints are rooted deep in the photosphere where no coronal disturbances can penetrate during the simulation. Therefore, the initial boundary conditions are,

$$\begin{aligned} \frac{\partial T}{\partial z} = v = \frac{\partial h}{\partial t} = 0 \quad \text{at} \quad z = L_h \\ T = 8 \times 10^3 K, \quad N = 8.255 \times 10^{13} \text{cm}^{-3}, \quad v = 0 \quad \text{at} \quad z = 0 \end{aligned} \quad (6.8)$$

z is the spatial coordinate axially round the loop from 0 at the footpoint to $1.2 \times 10^9 \text{cm}$ at the loop top, L_h . The plasma is assumed to be a fully ionised single temperature one i.e. $T_p = T_e$, except as regards the radiative power loss which is dominated by light ion emission. $N_e = N_p$ and $N_H = 0$.

The thermal heat flux equations only account for contributions from electrons and are modelled by the Spitzer-Harm expression, viz.,

$$q = \kappa_0 T_e^{5/2} \frac{\partial T_e}{\partial z} \quad (6.9)$$

with units of $\text{ergs cm}^{-2} \text{s}^{-1}$. This expression assumes that the coulomb logarithm is approximately 20 and $\kappa_0 = 9.203 \times 10^{-7}$. The radiative power loss is assumed to be that of an optically thin plasma and is given by,

$$R = N_e N_p \Omega(T_e) \quad (6.10)$$

where,

$$\Omega(T_e) = \begin{cases} 3 \times 10^{-22} \left(\frac{T_e}{2 \times 10^4} \right)^3, & T_e < 2 \times 10^5 K \\ 3 \times 10^{-22}, & 2 \times 10^4 \leq T_e < 2 \times 10^5 K \\ 3 \times 10^{-22} \left(\frac{T_e}{2 \times 10^5} \right)^{-1/2} + 2 \times 10^{-23} \left(\frac{T_e}{10^8} \right), & T_e \geq 2 \times 10^5 K \end{cases} \quad (6.11)$$

A geometrical configuration of the loop is accounted for by the imposition of a pseudo-gravitational term for the acceleration i.e.

$$g(z) = g_0 \sin \frac{\pi z}{2L_h} C \quad (6.12)$$

$$C = \left(\frac{R_0}{r(z)} \right)^2 \quad (6.13)$$

where the correction factor C takes account of the variation with distance from the solar centre over the height of the loop and g_0 is the gravitational acceleration at the surface of the Sun. This correction is only minor since the minimum value of C is at the loop top and equals 0.978.

The heating function for the loop consists of two parts i.e.

$$H = H_{init} + H_f \quad (6.14)$$

An ambient heating function, H_{init} , maintains the initially static model atmosphere by balancing the initial radiative losses. This is expressed as,

$$H_{init}(z) = \begin{cases} 9.01 \times 10^{-3}, & z > 2 \times 10^8 \text{ cm} \\ N_e^2 \Omega(T_{init}), & z < 2 \times 10^8 \text{ cm} \end{cases} \quad (6.15)$$

where T_{init} is the initial temperature at a given height, z. The static atmosphere is perturbed by an energy injection at the loop apex. The flare heating function, H_f , is

Gaussian with a source length $\sigma = 5 \times 10^8 \text{cm}$. The expression used is,

$$H_f(z, t) = \begin{cases} E \exp(-(z - L_h/\sigma)^2), & 0 < t < 5s \\ 0 & t > 5s \end{cases} \quad (6.16)$$

where the integral over the whole loop gives a total power of $2 \times 10^9 \text{ergscm}^{-2}\text{s}^{-1}$. In this test, we neglect the effects of viscosity and solve the plasma fluid equations of section.6.3.1.

As mentioned in section.6.2 one of the main difficulties is in resolving the steep temperature gradient that develops as a result of the flare injection. For this test we introduce the same *adaptive regridding* facility as originally defined by MacNeice (1983) in order to provide adequate spatial resolution and place it most advantageously. The method used was to construct the initial grid containing 250 points and initially place the finest resolution of $1.0 \times 10^4 \text{cm}$ at a height of $2 \times 10^8 \text{cm}$ where the starting temperature was $3 \times 10^4 \text{K}$. This is the lower transition zone boundary. The cell used was number 114. The grid cells expand uniformly away from this point with their size calculated to fill the rest of the loop. Thus we have two constant factors, one to describe the expansion up the loop into the corona and another to describe the expansion down into the chromosphere, the largest variation between neighbouring cells being 8%. At each integration timestep the temperature profile is checked in the region $3 \times 10^4 \text{K}$.

$$\left| \frac{T_{i+1} - T_i}{\min(T_{i+1}, T_i)} \right| < 1 \quad (6.17)$$

The constraint of equation.6.17 was applied and a check was made to ensure that the temperature of $3 \times 10^4 \text{K}$ was found within three cells of number 114. T_i denotes the temperature at the i th cell. If the temperature gradient is inadequately resolved or the cell has moved sufficiently then rezoning of the grid takes place. The minimum cell size required to satisfy equation.6.17 is calculated and placed at the height of the cell where the temperature of $3 \times 10^4 \text{K}$ is located. The grid is then reconstructed using the same method as above, with new expansion factors calculated. Thus the grid rezones only when it is required and unnecessary computations are avoided.

Timestep splitting techniques are employed to solve terms in the equations only over the timescales on which they vary. Thus conductive, radiative power loss and

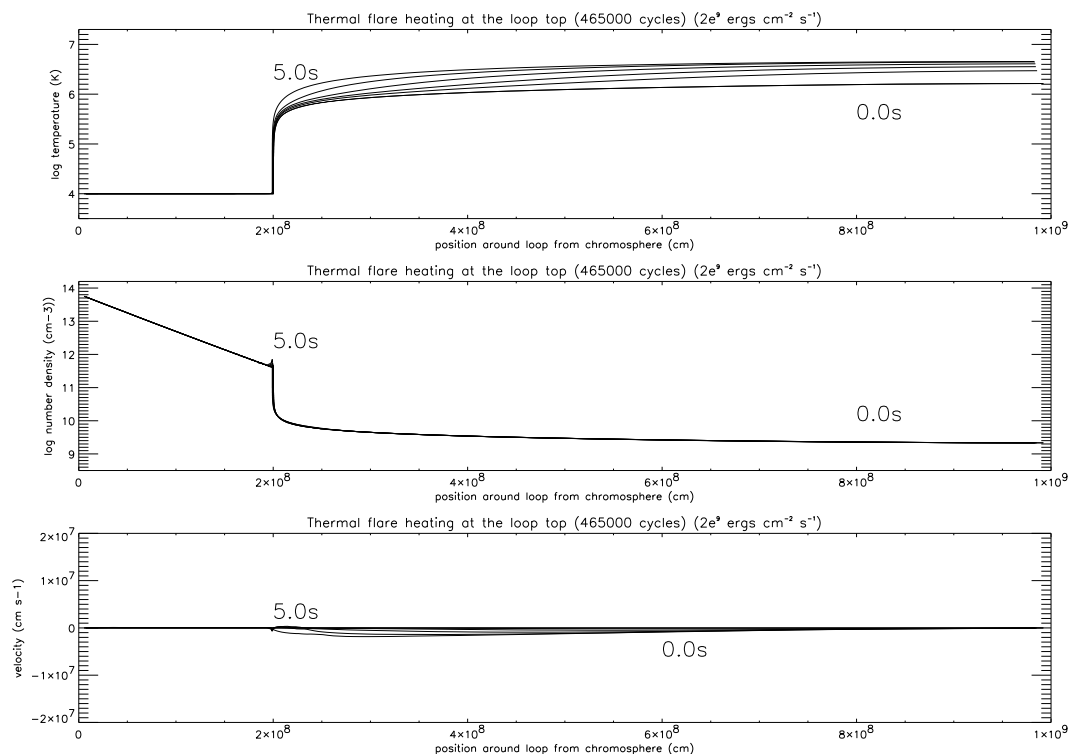


Figure 6.1: Temperature, density and velocity plots against position around the loop from the lower chromosphere as a function of time.

hydrodynamic terms are solved individually for example. More details are given by MacNeice(1983). Of course this helps in computational efficiency but is not so critical nowadays due to great advances in computational processing speeds.

Test Comparison

The results of the modified benchmark test run are given in figs. 6.1 and 6.2. The results satisfactorily reproduce those of MacNeice(1986) albeit within a shorter timescale due to the decrease in loop size and consequent increase in range and deposition of the energy distribution. Figure.6.1 shows the results for the first 5 secs and figure. 6.2 the subsequent development, around the transition region boundary, until termination of the calculation at 7.2 secs. The expected conduction front

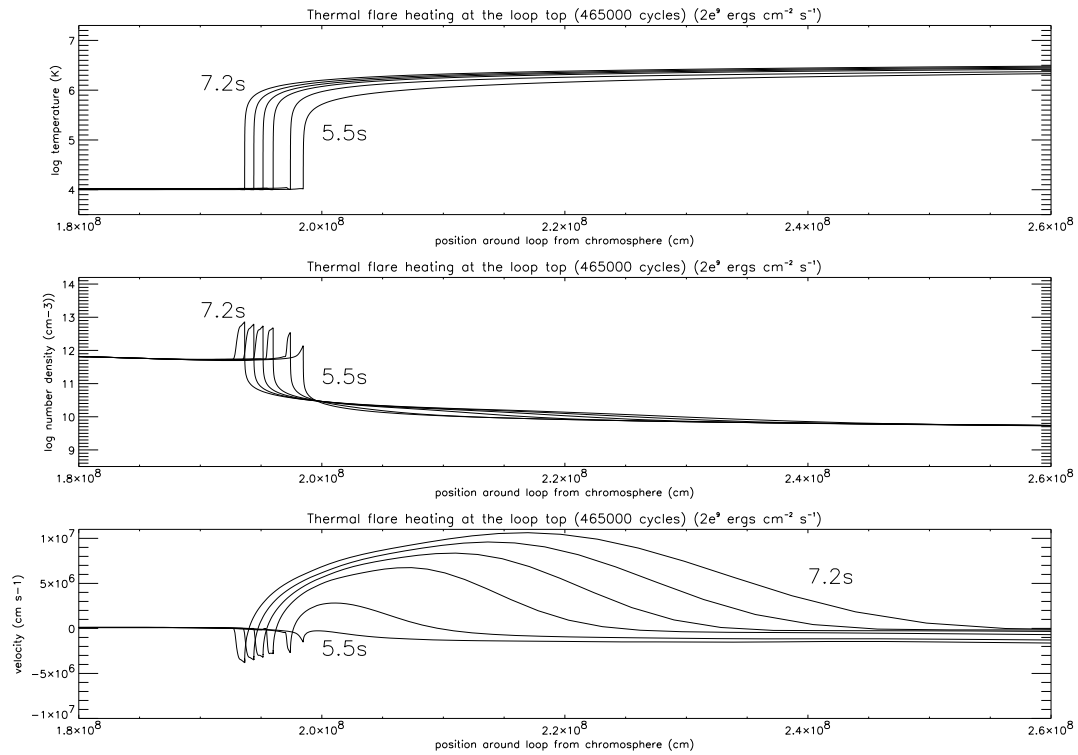


Figure 6.2: Temperature, density and velocity plots against position around the loop from the lower chromosphere as a function of time.

develops and moves down towards the transition region arriving there in under 5 secs. The coronal plasma expands downwards at a velocity of $\sim 2 \times 10^6 \text{ cm s}^{-1}$. From fig.6.2 we see that the expected pressure enhancement does indeed develop and causes plasma motions both up and down the loop. The transition region begins to progress downward and pushes material ahead of it in a compression front. Due to considerations of momentum conservation and since the upward ablation of material has a larger velocity, a much larger mass of material is involved in this downward chromospheric compression. The upward evaporation accelerates quickly reaching a velocity of $\sim 1.0 \times 10^7 \text{ cm s}^{-1}$ at the expansion front after 7.2s. The width of the chromospheric compression grew slightly as it progressed reaching about $\sim 9 \times 10^5 \text{ cm}$ by the end of the simulation with a peak density of $\sim 6 \times 10^{12} \text{ cm}^{-3}$. The temperature

at the loop top was $\sim 3.2 \times 10^6 K$. The temperature gradient of the transition region continually steepened to cope with the conducted heat flux from the corona. As a result the minimum grid cell size fell rapidly below 16cm requiring very short integration timesteps of $\sim 7 \times 10^{-7}$ s. The computational resources available today are certainly improved compared to those available to MacNeice(1986). For example, in MacNeice(1986) his resources could no longer support the calculation once the grid size had fallen below 30cm and the integration timestep below 10^{-5} s. This in itself is less of a problem for us, we worked consistently at integration timesteps nearly two orders of magnitude smaller. However, the calculation eventually failed as it was unable to reconstruct the grid. The code uses a Newton-Raphson convergence scheme to calculate the grid expansion factors. In our test the scheme never converged. This problem should easily be overcome by an additional check in the program. That is, if the scheme does not converge after, say, 100 attempts, the expansion variables are taken from the previous cycle. This method is less accurate but should allow the computation to continue.

6.4 Applications to Quiet Sun Activity

The adaptive rezoning capabilities of the hydrodynamic model have proven effective in resolving shock fronts and extremely violent flare behaviour. We intend to adapt this model, by imposition of pseudo-gravity and alternative energy injections, to investigate the energy balance of coronal prominence condensation models (see for example Antiochos & Klimchuk(1991)) and impulsive bursts (see Spadaro et al.(1996)). We have undertaken some preliminary analysis of what is required and have some suggestions to offer here.

Antiochos & Klimchuk (1991) proposed a model for the formation of prominence condensations. They argued that a localized heating at the base of a coronal loop could form a condensation around the loop midpoint if the loop they considered was initially static with a shallow dip at the apex. The geometry of the loop was that of a semi-circle attached to a broad inverted Gaussian. Such a loop magnetic field configuration was imposed by a pseudo-gravitational term which can easily be

incorporated into our own code. The key idea was based on the expected response of the chromosphere to the localised heating. As with numerical simulations of flares (e.g. section.6.3.1), they anticipate that chromospheric evaporation causes material to rise up the loop and essentially become suspended in the shallow dip forming a cool dense condensation. The results of their simulations bore this out. However, their calculation terminated due to the formation of a steep temperature gradient around the edge of the dip in a transition region between the coronal material and the condensation. This was outside of the range of the finest resolution of their grid which they judged correctly would be required at the transition region itself.

Clearly there are a number of areas that we can immediately and speedily address. On the hydrodynamic side, imposition of the same geometric/gravitational configuration as that of Antiochos & Klimchuk (1991) and modification of the location and form of the transient heating source can be done easily. The development of a ‘second’ transition region requires an adaptive grid to calculate the required spatial resolution and place it correctly. This is already an inherent part of our code (see section. 6.3.1). It is our intention to construct a *double adaptive* grid that allows us to check the temperature gradient both above and below the maximum height of the loop. Thus we will be able to track the development of the condensation until it reaches approximately the width of observed condensations ($\sim 1000km$), something Antiochos & Klimchuk were unable to do.

On the atomic side, combining the model with ADAS will allow us to link effective emissivity coefficients with the time development of density, temperature and velocity data around the loop for observation prediction. There are several datasets relating to the connection between eruptive prominences and coronal mass ejections already available from SOHO and these should be of use in this respect. The formation of the cool dense condensation also raises the question of optical thickness effects. Through the study of opacity with the CDS & SUMER spectrometers our group has built up some expertise on excited population modelling for optically thick circumstances and simple escape factor treatments of photo-absorption. This should allow much progress to be made in probing the radiation emission of prominence condensations.

A preliminary analysis of the possibility of modifying the code to simulate impulsive bursts highlighted difficulties. Although alteration of the energy injection term proved easy it was not possible to match the magnitude and duration of observed bursts realistically. For example, a typical input energy rate for micro-flares is ~ 10 ergs $\text{cm}^{-3} \text{s}^{-1}$ with a duration of $\sim 0.7 \text{s}$ (Spadaro & Lanza(1995) - private communication). Thus a total pulse of 1.7×10^{23} ergs was injected at the footpoint of an initially static semi-circular symmetric loop (essentially the same as used in section. 6.3.1) for our test. This had no noticeable effect on the hydrodynamic evolution of the loop as it was smaller than the ambient heating function. This result may have been anticipated as micro-flares are essentially a candidate for a mechanism that purports to be responsible for coronal heating. Since our hydrodynamic model is initially that of a static atmosphere we effectively take due account of the coronal heating mechanism without defining what it is. This problem requires further attention.